PERFORMANCE EVALUATION OF ACTIVE CONTOUR MODELS FOR CAROTID PLAQUE SEGMENTATION

C.P. Loizou*, C.S. Pattichis**, M. Pantziaris***, A. Nicolaides ****

* Intercollege, Dept. of Computer Science, P. O. Box 51604, CY-3507 Limassol, Cyprus
** Dept. of Computer Science, University of Cyprus
*** Cyprus Institute of Neurology and Genetics, Nicosia, Cyprus
**** Dept. of Vascular Surgery, Imperial College London, U.K

christosl@lim.Intercollege.ac.cy

Abstract: In this paper we compare four different snakes segmentation methods for segmenting the athrerosclerotic carotid plaque from longitudinal ultrasound images of the carotid artery. The accuracy and reproducibility of the methods were tested on 80 images and the results were compared with the manual delineations of an expert. The comparison showed that the Lai&Chin snakes segmentation method gave better results with the true positive fraction, TPF, true negative fraction TNF, Williams index, KI, and overlap index, to be 82.70%, 80.89%, 80.66%, and 69.30% respectively. Better false negative fraction, FNF, and false positive fraction, FPF, were given by the Balloon method with 13.90% and, 5.40% respectively.

Introduction

Carotid atherosclerosis is the primary cause of stroke and the third leading cause of death in the United States. Almost twice as many people die from cardiovascular diseases than from all forms of cancer combined. Atherosclerosis is a disease of the large and medium size arteries, and it is characterized by plaque formation due to progressive intimal accumulation of lipid, protein, and cholesterol esters in the blood vessel wall [1], which reduces blood flow significantly. Traditionally the degree of artery stenosis, or narrowing, has been targeted as the marker for assessment of risk for plaque vulnerability depended on the type of plaque, and considered to cause either a complete arterial occlusion or ischemic event in the brain. The risk of stroke increases with the severity of carotid stenosis and is reduced after carotid endarterectomy [2]. The degree of internal carotid stenosis is the only well established measurement that is used to assess the risk of stroke [3]. Indeed, it is the only criterion at present used to decide whether carotid endarterectomy is indicated or not [4].

The development and testing of new, accurate methods, for non-invasive assessment of plaque size and vulnerability will help the clinical assessment of the subject. Furthermore, non-invasive assessment of plaque characteristics will help the way in which athrerosclerotic disease is diagnosed, monitored and treated.

Active contour models have been proven to be a promising approach in many different fields in computer vision [5]. They have been applied to image segmentation, analysis of static images [6] and image sequences of real time systems [7]. Many extensions of the original snake approach [5] have been suggested, referring to the definition of the energy as well as to the energy minimization and some regularization factors for the snake [8]. The models have been presented in different application areas thus making comparisons or predictions of the behavior of the models in another area of application hardly to draw.

The research on plaque segmentation of carotid artery ultrasound images presented in the literature, is very limited. This is also shown from the small number of publications made in this area, which are mostly reported in conference proceedings. Specifically, in [9] an unknown number of transversal ultrasound images of the carotid artery were used to detect the lumen borders of the carotid artery. The proposed method consisted of four stages, namely pre-processing, quantization, morphological contour detection, and contour enhancement. In the pre-processing step a histogram equalization was performed, and a median filter was applied for despeckling the image. In [10] a dynamic balloon model [7] represented by a triangular mesh was applied for detecting the plaque borders on two 3D ultrasound carotid images where the initial contour was placed manually. The plaque borders were detected through reconstruction of the inner lumen borders. The result was a surface indicating the outline of the lumen. In other studies performed researchers have tested their proposed segmentation techniques, on 20 MRI transversal carotid images [11] to detect the lumen and the outer wall boundaries of the artery by using the gradient vector flow (GGVF) field [12], where the snake initial contour was placed manually by an expert. In [13], a segmentation method for the arterial walls and plaque based on dynamic programming was proposed. The method was applied on 62 transversal MRI images and compared with the manual delineations made by an expert whereas the initial contour was found by manually placing four points on the artery walls.

There is until today no other study reported for comparing different snake models for segmenting longitudinal ultrasound images of the carotid artery,

ISSN: 1727-1983

which will enable us to choose the optimal active contour model.

In this paper we investigate the segmenation of atherosclerotic carotid plaque using four different active contour models as follows: (i) the Williams&Shah snake [6], after the addition of some constrains [9], (ii) the Balloon [7], (iii) the Lai&Chin [8], and (iv) the gradient vector flow (GVF) snake [12]. Preliminary results of this study were published in [14] and [15]. The snake segmentation methods as well as the methodology of our study is presented in the following section. Finally, the results and the concluding remarks are presented.

Methods

Williams&Shah Snake

A snake contour may be represented parametrically by $v(s) = [x(s), y(s)]$, where $(x, y) \in \Re^2$ denotes the spatial coordinates of an image, and $s \in [0,1]$ represents the parametric domain. The snake adapts itself by a dynamic process that minimizes an energy function defined as [6]

$$E_{snake}(v(s)) = E_{\text{int}}(v(s)) + E_{image}(v(s)) + E_{external}(v(s)) = \int_s (\alpha(s)E_{cont} + \beta(s)E_{curv} + \gamma(s)E_{image} + E_{external})ds. \quad (1)$$

At each iteration step, the energy function in (1), is evaluated for the current point in $v(s)$, and for the points in an mxn neighborhood along the arc length, s, of the contour. Subsequently the point on $v(s)$, is moved to the new position in the neighborhood that gives the minimum energy. The term $E_{\text{int}}(v)$, in (1) denotes the internal energy derived from the physical characteristics of the snake and is given by the continuity $E_{cont}(v)$, and the curvature term $E_{curv}(v)$. This term controls the natural behavior of the snake. The internal energy contains a first-order derivative controlled by $\alpha(s)$, which discourages stretching and makes the model behave like an elastic string by introducing tension and a second order term controlled by $\beta(s)$, which discourages bending and makes the model behave like a rigid rod by producing stiffness. The weighting parameters $\alpha(s)$ and $\beta(s)$ can be used to control the strength of the model's tension and stiffness, respectively. Altering the parameters α, β, and γ, affect the convergence of the snake. The second term in (1) E_{image}, represents the image energy due to some relevant features such as the gradient of edges, lines, regions and texture [6]. It attracts the snake to low-level features such as brightness and edge data. Finally the term $E_{external}$, is the external energy of the snake, which is defined by the user and is optional. In our study we used a modification of the greedy algorithm as presented in [6].

Balloon Snake

Cohen [7] introduced a Balloon snake, whose internal energy causes it to expand from inside of the boundary until it reaches it. The original snake model was improved through normalization of the force field term. The energy functional in (1) may then be rewritten by substituting the image field force, E_{image}, as follows

$$F_{image} = -\frac{k\nabla E_{image}}{\left\|\nabla E_{image}\right\|} = k_1 n(s) - k_2 \frac{\nabla E_{image}}{\left\|\nabla E_{image}\right\|}, \quad (2)$$

where $n(s)$, is a normal unity vector normal to the snake curve at point $v(s)$, and k_1, is the amplitude of this force. The addition of a new term, $k_1 n(s)$, to the force field, F_{image}, makes the contour have a more dynamic behavior. The curve may be considered as a balloon that is inflated. By changing the sign of, k_1, the curve will deflate instead of inflate.

Lai&Chin Snake

Lai&Chin proposed a different snake approach, including a regularization parameter, λ_π, to control the balance between the external and the internal forces [8]

$$E_{snake}(v(s)) = \int_{s=0}^{1} \{\lambda_\pi E_{\text{int}}(v(s)) + (1-\lambda_\pi)E_{image}(v(s))\}ds. \quad (3)$$

If, the regularization parameter, $\lambda_\pi = 1$, then the snake uses the internal energy only, whereas if, $\lambda_\pi = 0$, the snake will be attracted to the selected image function only. The regularization parameter is calculated at contour points as [8]

$$0 < \lambda_{\pi i} = \frac{\sigma_n^2}{\sigma_i^2 + \sigma_n^2} < 1, \quad (4)$$

where σ_i^2, is the variance of the snake point i, and σ_n^2, the variance of the noise at the snake point.

GVF Snake

In a GVF snake model [12], the external force cannot be written as the negative gradient of a potential function. Instead, the external force of the GVF snake model is defined by a gradient vector flow field, which minimizes the energy functional given by

$$E_{snake}(v(s)) = \iint \mu(u_x^2 + u_y^2 + v_x^2 + v_y^2) + \left|\nabla g^2\right| g - \nabla g\Big|^2 dxdy \quad (5)$$

The notation g, and μ, stands for an edge map computed using the image, and a regularization parameter, respectively. The GVF field is obtained directly by solving numerically the Euler equations [12]. The position of the GVF snake is changed iteratively such that the energy functional in (4) is minimized.

The parameter values for the snake models, were the same in all experiments, namely for the

ISSN: 1727-1983

Williams&Shah snake, $\alpha_s = 0.4$, $\beta_s = 0.4$, $\gamma_s = 2$, the elasticity, rigidity and the regularisation parameters for the GVF snake was, $\alpha_{GVF} = 0.05$, $\beta_{GVF} = 0$, $\mu_{GVF} = 0.2$, and the regularisation parameter λ_π, for the Lai&Chin snake, was variable and calculated according to (4).

Recording of Ultrasound Images

A total of 80 B-mode and blood flow longitudinal ultrasound images of the common carotid artery (CCA) bifurcation were selected at random representing different types of atherosclerotic plaque formation with irregular geometry typically found in this blood vessel. The images were captured using the ATL HDI-5000 ultrasound scanner [16] and were recorded digitally on a magneto optical drive, with a resolution of 768x756 pixels with 256 gray levels. The image resolution was 16.66 pixels/mm.

The ATL HDI-5000 ultrasound scanner is equipped with an 256-element fine pitch high-resolution 50 mm linear array, a multi element ultrasound scan head with an extended operating frequency range of 5-12 MHz and real spatial compound imaging. The scanner increases the image clarity using SonoCT imaging by enhancing the resolution and borders, so that interface margins can be displayed better.

Traditionally, suspected plaque formation is confirmed using color blood flow imaging. The PW Doppler used can detect blood flow at a specific depth by selecting the time interval between the transmitted and received pulses. In this work we used the blood flow image obtained for an initial snake contour estimation. The limitations of this approach i.e. using the blood flow image to locate the blood borders are the following: a) the blood sometimes hides areas of the tissue (reverberations), and b) the colour does not always fill up the places where blood has a low speed.

Plaques may be classified into the following types: type I: uniformly echolucent (black), where bright areas occupy less than 15% of the plaque area, type II: mainly echolucent, where bright echoes occupy 15-50% of the plaque area, type III: mainly echolucent, where bright echoes occupy 50-85% of the plaque area, type IV: uniformly echogenic, where bright echoes occupy more than 85% of the plaque area, type V: calcified cup with acoustic shadow so that the rest of the plaque cannot be visualized [4], [17]. In this study the plaques delineated were of type II, III and IV because it is easier to make a manual delineation since the fibrous cup, which is the border between blood and plaque, is more easily identified. If the plaque is of type I, borders are not visible well. Plaques of type V produce acoustic shadowing and the plaque is also not visible well. Plaques of type I and V were therefore not delineated in our study.

Image Normalization

The images were normalized manually by adjusting the image linearly so that the median gray level value of blood was 0-5, and the median gray level of adventitia (artery wall) was 180-190 [4]. The scale of the gray level of the images ranged form 0 to 255. This normalization (i.e. using blood and adventitia as reference points) was necessary in order to extract comparable measurements in case of processing images obtained by different operators or different equipment [4], [17].

Manual Delineation of Plaque

One vascular expert delineated the plaques on all 80 B-mode ultrasound images of the carotid artery after image normalization. The expert defined the outline of the plaque by marking 20 to 40 consecutive points on the plaque border on the B-mode image. In order to delineate the plaque on the B-mode image the expert was guided by the blood flow image.

The plaque outline was drawn on the far wall (posterior) of the CCA because there, the intima media complex and the neighboring tissues are more visible. Delineations taken from the near wall are less accurate, because of overlap of echo pulses, and therefore less reproducible than those taken from the far wall [4], [17].

Despeckling

Speckle is a form of multiplicative noise, which corrupts medical ultrasound imaging making visual observation difficult. In a recent study [18] we have shown that despeckle filtering improves the experts optical perception. Many researchers refer to speckle as the major difficulty in analyzing and segmenting ultrasound images [18]-[21]. In this study, the linear filter *lsmv* was used, which may be described by a weighted average calculation using sub region statistics to estimate statistical measures over pixel windows [18] (typically 5x5, 7x7, or 9x9 sliding pixel windows). It assumes that the speckle noise model has the following multiplicative form [18]

$$g_{i,j} = f_{i,j} n_{i,j} \text{ with } i, j \in N, \quad (6)$$

where $g_{i,j}$, represents the noise pixel in the middle of the moving window, $f_{i,j}$, represents the noise-free pixel and $n_{i,j}$, is a Rayleigh distributed noise on pixel. Hence the equation in this class may be traced back to the following equation [18]

$$f_{i,j} = \bar{g}_{i,j} + k_{i,j}(g_{i,j} - \bar{g}) \quad (7)$$

where $f_{i,j}$, is the new estimated noise free pixel value, $g_{i,j}$ is the noisy pixel value in the moving window surrounding and including pixel $g_{i,j}$, $\bar{g}$ is the local mean value of an MxN region, $k_{i,j}$ is a weighting factor with $k \in [0..1]$, and i, j are the absolute pixel coordinates. The factor $k_{i,j}$ is a function of the local statistics in a moving window. It can be found in the literature and may be derived as [21]

$$k_{i,j} = \sigma_g^2 / (\bar{g}^2 \sigma_g^2 + \sigma_n^2) \quad (8)$$

ISSN: 1727-1983

where σ_g^2, and σ_n^2, represents the variance in the moving window and the variance of noise in the whole image, respectively [18]. The noise variance may be calculated for the logarithmically compressed image, by computing the average noise variance over a number of windows with dimensions considerable larger than the filtering window. In each window the noise variance is computed as [19]

$$\sigma_n^2 = \sum_{i=1}^{p} \sigma_p^2 / \overline{g}_p \qquad (9)$$

where σ_p^2, and $\overline{g}_p$, are the variance and mean of the noise in the selected windows respectively and p, is the index covering all windows in the whole image [19]. If the value of $k_{i,j}$, is 1 (in edge areas) this will result to an unchanged pixel, whereas a value of 0 (in uniform areas) replaces the actual pixel by the local average, $\overline{g}$, over a small region of interest (see (7)). The moving window used for this study was 5x5.

Snake Contour Initialization

It is importnat to position the initial snake contour as close as possible to the area of interest otherwise the snake may be trapped into local minima or false edges, and converge in a wrong location. We have therefore developed an initialization procedure where the outline of the blood flow is used to detect the initial contour placement [9]. The initialisation procedure may be described as follows (see also Fig. 1): a) Cross correlate the B-mode image (see Fig. 1a) with the blood flow image (see Fig. 1b) and extract the blood flow area. b) Dilate the extracted blood flow area to close small gaps and remove small regions. c) From the dilated blood flow image, detect the blood flow edge contour (see Fig. 1c). d) Mark a region of interest on the edge contour (task carried out by the expert, rectangle shown in Fig. 1c), where the lower or upper boundary of plaque is covered to use it as initial snake contour. e) Sample the initial snake contour at 20 to 40 consecutive snake points to construct an interpolating B-spline (see Fig. 1d). f) Connect the first and the last snake points on the initial contour to form a close contour. g) Despeckle the B-mode image by the *lsmv* filter. h) Map the initial plaque contour on the B-mode image. i) Deform the initial contour by a snake to accurately locate the plaque-blood borders, and j) Save the final plaque contour and display it on the B-mode image (see Fig. 1f).

Evaluation of the Segmentation Methods

To evaluate the performance of the four snakes segmentation methods, we compared the snakes segmented borders with the manually outlined borders defined by an expert. The intra- and inter-observer

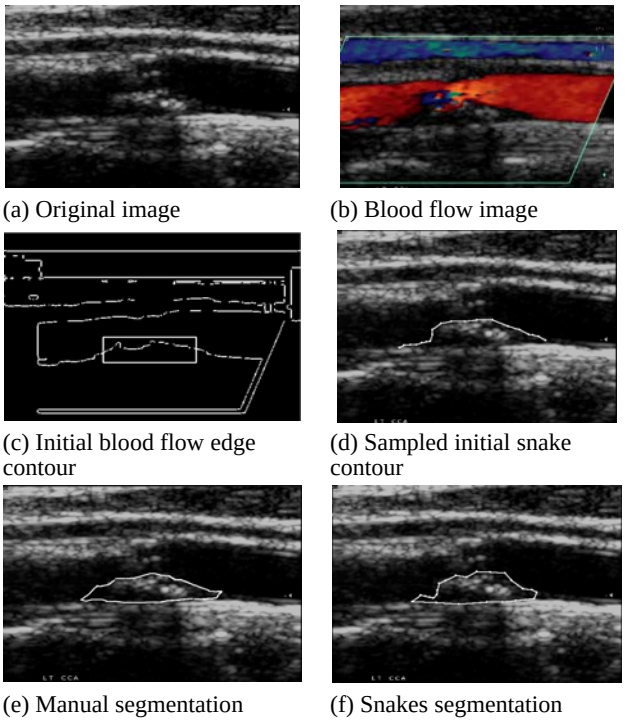

(a) Original image (b) Blood flow image

(c) Initial blood flow edge contour (d) Sampled initial snake contour

(e) Manual segmentation (f) Snakes segmentation

Figure 1: (a) Original ultrasound image of a carotid artery with plaque, (b) blood flow image, (c) initial blood flow edge contour with expert selected area for the initial contour, (d) sampled initial snake contour, (e) manual segmentation of plaque, and (f) Snakes segmentation of plaque.

variability caused by multiple experts, was not taken into account in this study. Let GT, denote the segmented area, representing ground truth, $\overline{GT}$, its complement, and AS the segmented area, obtained by the computerized approach. The receiver operating characteristics (ROC) analysis [22] was used to assess the specificity and sensitivity of the method by the true-positive fraction, TPF, and false-positive fraction, FPF, detected [21] respectively. The TPF, is calculated when the expert detects a plaque (when plaque is present) and the computerized method identifies it as so, whereas the FPF, is calculated when the expert detects no plaque and the computerized method incorrectly detects that there is plaque present. The TNF fraction is calculated when the expert identifies no plaque and the computerized method identifies it as so (absent), whereas the FNF is calculated when the expert identifies plaque presence and the computerized method incorrectly identifies plaque absence. Ratios of overlapping areas, can also be assessed by applying the similarity kappa index, KI, [23], and the overlap index [24]. These indices were computed as follows

ISSN: 1727-1983

$$TPF = \frac{AS \cap GT}{GT}, \quad FPF = \frac{|AS - GT|}{\overline{GT}},$$
$$KI = 2\frac{GT \cap AS}{GT + AS}, \quad overlap = \frac{GT \cap AS}{GT \cup AS} \qquad (10)$$

where $\cap$ denotes the intersection and $\cup$ the union of the two areas. The intersection gives the probability that both AS and GT occur and the union is the probability that either AS or GT occur.

Results

Figure 2 illustrates the original longitudinal ultrasound B-mode image of the carotid artery with a manual delineation made by an expert in (a), and the results of the Williams&Shah snakes segmentation in (b), the Balloon segmentation in (c), the Lai&Chin segmentation in (d), and the GVF segmentation in (e).

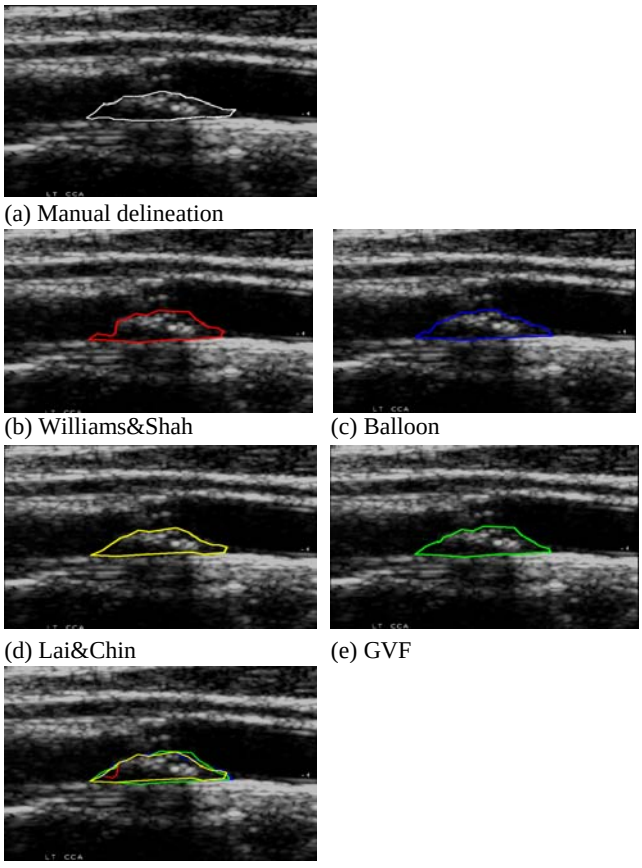

(a) Manual delineation

(b) Williams&Shah (c) Balloon

(d) Lai&Chin (e) GVF

(f) Segmentation contours computed in (b)-(e) superimposed

Figure 2: Segmentation results on a longitudinal ultrasound B-mode image of the carotid artery with plaque, with: (a) manual segmentation, (b) Williams&Shah, (c) Balloon, (d), Lai&Chin, (e) GVF snake, and (f) segmentation contours computed in (b)-(e) superimposed.

Figure 2f shows the segmentation contours computed in Fig. 2b-2e superimposed on the same image. As shown the manual and the snakes segmentation results are visually very similar suggesting that all four snakes segmentation methods can be interchangeable. Furthermore, when superimposing all segmentation results (see Fig. 2f) it is shown that the differences between all four snakes segmentation methods are very small. The best segmentation results were obtained by the Lai&Chin method (yellow line), which is closer to the manual segmentation result followed by the traditional snake (red line). Balloon and GVF yielded similar accuracy of the plaque segmentation, however GVF has a better ability to fill boundary concavities. The Balloon snake inflates and moves far away form the actual object in many cases. The Balloon model may identify smooth regions, especially when the initial snake contour is very close to the actual object of interest. Furthermore, the Balloon also inflates in many cases and moves far away from the object of interest, thus failing to identifies correctly image concavities.

Table 1: ROC Analysis for the Four Different Plaque Segmentation Methods and the Manual Delineations Made by an Expert on 80 Ultrasound Images of the Carotid Artery

Segmentation Method	System Detects	Expert Detects no plaque (%)	Expert Detects plaque (%)	KI (%)	Overlap Index
Williams& Shah	No plaque	TNF=77.6	FNF=19.6	78.9	67.6
	Plaque	FPF=6.5	TPF=81.8		
Balloon	No plaque	TNF=77.1	**FNF=13.9**	77.9	67.8
	Plaque	**FPF=5.4**	TPF=80.4		
Lai&Chin	No plaque	**TNF=80.9**	FNF=15.6	**80.7**	**69.3**
	Plaque	FPF=5.9	**TPF=82.7**		
GVF	No plaque	TNF=79.4	FNF=14.9	77.3	66.6
	Plaque	FPF=6.3	TPF=79.6		

Table 1 presents a comparison of the four different plaque segmentation methods, with the manual segmentation, as performed by an expert, on 80 ultrasound images of the carotid plaque. The results showed that the Lai&Chin segmentation method, agrees with the expert in 80.9% of the cases, TNF, by correctly detecting no plaque, in 82.7% of the cases, TPF, by correctly detecting a plaque, disagrees with the expert in 15.6% of the cases, FNF, by detecting no plaque, and in 5.9% of the cases, FPF, by detecting a plaque. The similarity kappa index, KI, and the overlap index, for the Lai&Chin snakes segmentation method were the highest, equal to 80.7% and 69.3% respectively. The best FPF, and FNF, fractions were given by the Balloon snakes segmentation method with 5.4% and 13.9% respectively. The GVF method showed for this experiment the worst results with the lowest similarity kappa index, KI (77.3%), and the lowest overlap index (66.6%).

Concluding Remarks

The results of this study showed that the segmentation method of Lai&Chin is the most appropriate to segment the plaque from ultrasound longitudinal images of the carotid artery after despeckle filtering with the *lsmv* filter and after image normalisation.

The method presented in this dissertation, is to the best of our knowledge the first computerized

ISSN: 1727-1983

approach for plaque segmentation in longitudinal ultrasound images of the carotid artery. Such a computerized method cannot only reduce significantly the time required for the image analysis, but also it can reduce the subjectivity that accompanies manual delineations and measurements. The method will be further evaluated on a larger number of ultrasound images and on multiple experts evaluation. Furthermore, it is expected that the segmentation method will be incorporated into an integrated system enabling the texture analysis of the segmented plaque, providing an automated system for the early diagnosis and the assessment of the risk of stroke.

Acknowledgment

This work was partly funded through the project *Integrated System for the Evaluation of Ultrasound Imaging of the Carotid Artery (TALOS)*, of the Program for Research and Technological Development 2003-2005, of the Research Promotion Foundation of Cyprus.

References

[1] ZARINS C.K., XU C., GLAGOV S. (1995): 'Atherosclerotic Enlargement of the Human Abdominal Aorta', (Elsevier Sc. Ireland), p.157-164.

[2] ACAS clinical advisory (1994): 'Carotid Endarterectomy for Patients with Asymptomatic Internal Carotid Artery Stenosis', *Stroke*, **25**, **12**, pp. 2523-2524.

[3] EXECUTIVE COMMITTEE FOR THE ASYMPTOMATIC CAROTID ATHEROSCLEROSIS STUDY (2002): 'Endarterectomy for Asymptomatic Carotid Stenosis', *J. Am. Med. Assoc.*, **273**, pp.1421-1428.

[4] NICOLAIDES A. et al. (2003): 'The Asymptomatic Carotid Stenosis and Risk of Stroke Study', *Int. Angiol.*, **22**, **3**, pp. 263-272.

[5] KASS M., WITKIN A., and TERZOPOULOS D. (1988): 'Snakes: Active Contour Models', *Int. Journal Compt. Vision*, **1**, pp. 321-331.

[6] WILLIAMS D., and SHAH M. (1992): 'A Fast Algorithm for Active Contour and Curvature Estimation', *GVCIP: Imag. Und.*, **55**, **1**, pp. 14-26.

[7] COHEN L.D. (1991): 'On Active Contour Models and Balloons', *Computer Vision, Graphics, and Image Processing: Image Understanding (CVGIP:IU)*, **53**, **2**, pp. 211-218.

[8] LAI K.F., and CHIN R.T. (1995): 'Deformable Contours-Modeling and Extraction', *IEEE Trans. on PAMI*, **17**, **11**, pp. 1084-1090.

[9] HAMOU A., EL.-SAKKA M. (2004): 'A Novel Segmentation Technique for Carotid Ultrasound Images', *Int. Conf. on Acoustic Speech and Signal Processing*, ICASSP 2004, p. III-521-III-524.

[10] GILL J.D. et al. (2000): 'Segmentation of Ulcerated Plaque: A sSemi-Automatic Method for Tracking the Progression of Carotid Atherosclerosis', World congress on Med. Phys. Biomed. Eng., Chicago, IL, p. 1-4.

[11] ADAMS G.J., VICK G.W., BALLANTYNE C.M., INSULL W., MORRISETT J.D. (2002): 'Estimation of Carotid Atherosclerotic Plaque Volume in Vivo Magnetic Resonance Images', Proc. EMBS/BMES Conf., p. 1072-1073.

[12] XU C., and PRINCE J. (1998): 'Generalized Gradient Vector Flow External Forces for Active Contours', *Signal Processing*, **71**, pp. 131-139.

[13] YANG F., HOLZAPFEL G.A., SCHULZE-BAUER CH. A.J., STOLLBERGER R., THEDENS D., BOLINGER L., STOLPEN A., and SONKA M. (2003): 'Segmentation of Wall and Plaque in in-vitro Vascular MR Images', *The Int. J. of Cardiovascular Imaging*, **19**, pp. 419-428.

[14] LOIZOU C.P. et al. (2004): 'Atherosclerotic Carotid Plaque Segmentation', Proc. of the 26th Annual Int. Conf. IEEE EMBS, San Francisco, California, USA, p. 1403-1406.

[15] LOIZOU C.P. (2005): 'Ultrasound image analysis of the carotid artery', Ph.D. dissertation, Kingston University, London, UK.

[16] A Philips Medical System Company, 'Comparison of image clarity, SonoCT real-time compound imaging versus conventional 2D ultrasound imaging', ATL Ultrasound, Report, 2001.

[17] ELATROZY T., et al. (1998): 'The Effect of B-mode Ultrasonic Image Standardization of the Echodensity of Symptomatic and Asymptomatic Carotid Bifurcation Plaque', *Int. Angiol.*, **17**, **3**, pp. 179-186.

[18] LOIZOU C.P. et al. (2005): 'Comparative Evaluation of Despeckle Filtering in Ultrasound Imaging of the Carotid Artery', *IEEE Trans. Ultrasonics Ferroelectrics and Frequency Control*, accepted, 2005.

[19] DUTT V. (1995): 'Statistical Analysis of Ultrasound Echo Envelope', Ph.D. Dissertation, Mayo Graduate School, Rochester, MN.

[20] Loizou C.P., Pattichis C.S., Istepanian R.S.H., Pantziaris M. (2004): 'Intima Media Segmentation of the Carotid Artery', IEEE Int. Conf. Medicon, X Medit. Conf. on Medical and Biological Eng., Ischia, Naples-Italy,POS-03, 499, p. 1-4.

[21] LEE J.S. (1981): 'Speckle Analysis and Smoothing of Synthetic Aperture Radar Images', *Comp. Graph. and Image Proc.*, **17**, pp. 24-32.

[22] METZ C. (1978): 'Basic Principles of ROC Analysis', *Semin. Nucl. Medic.*, **8**, pp. 283-298.

[23] ZIJDENBOS A. et al. (1994): 'Morphometric Analysis in White Matter Lesions in MR Images: Method and Validation', *IEEE Trans. Med. Imag.*, **13**, **4**, pp. 716-724.

[24] KELEMEN A., SZEKELY G., and GERIG G. (1999): 'Elastic Model-Based Segmentation of 3-D Neuroradiological Data sets', *IEEE Trans. Med. Imag.*, **18**, **10**, pp. 828-839.

ISSN: 1727-1983